Ultraviolet Network Coverage Based on Non-Line-of-Sight Channel

Cheng Li, Zhiyong Xu, Jingyuan Wang, Jiyong Zhao, and Jianhua Li

***Abstract*—Ultraviolet (UV) networks, owing to their advantages of low eavesdropping rates, low background noise, strong anti-interference abilities, and non–line-of-sight (NLOS) communication, have high prospects for application in the complex electromagnetic environment. In this study, UV network coverage was systematically evaluated based on the NLOS channel. Combined with a designed node model and a specific communication mode, a two-dimensional network coverage model was established and expressions of network coverage area and connectivity were derived mathematically. Subsequently, the effects of the transceiver elevation combination, number of nodes, data rate, and transmission power on the network coverage performance were analyzed, and the communication parameters were optimized to match different network scenarios. The results show that the bigger the transceiver elevation combination, the more stringent the communication parameters required by the UV network coverage. Finally, a coverage evaluation experiment with four-node network was conducted. This study provides theoretical reference information for actual network deployment.**

***Index Terms*—Connectivity, coverage evaluation, UV network.**

I. Introduction

ULTRAVIOLET (UV) communication systems use the scattering of UV light in the atmosphere to realize information transmission [1]. They have the advantages of low eavesdropping rates, low background noise (owing to the 200–280 nm "solar-blind" band), strong anti-interference abilities, and non-line-of-sight (NLOS) communication [2], [3]. However, UV NLOS communication relies on scattering from aerosol particles in the atmosphere, leading to excessive path loss; and with the limitations of light power and photodetectors, the point-to-point communication distance is typically less than 500 m [4]. Therefore, combining UV communication with an ad hoc network to construct a UV network can expand the restricted-communication distance, meeting the requirements of covert communication. Such networks have high application prospects in secure communication (including military networks), emergency services, disaster recovery, and in other complex electromagnetic environments [5]. Unfortunately, high-power UV light sources cause damage to the eyes and skin; therefore, the power of the light source should be strictly controlled according to safety regulations.

Network coverage is a reference standard reflecting the quality of the communication service provided by a UV network, with goals including "coverage of the target area" and "multi-connectivity network" [6]. Coverage evaluation is the basis UV network research.

Zhao proposed a coverage optimization strategy based on a genetic algorithm to improve the coverage range of UV networks [7]. Ke et al. analyzed the effective coverage of UV networks based on the NLOS single scattering channel model [8]. However, these studies only discussed UV network coverage and did not include in-depth research on network connectivity.

Conversely, Vavoulas proposed that the communication parameters affecting the network connectivity primarily include transmission power, supported data rate, and error probability [9]. Under the random waypoint mobility model and circular movement-based node motion model [10], Zhao discussed the effects of communication parameters on UV network connectivity. However, the network model was built in a circular area and is not suitable for more general scenarios.

In this study, we systematically analyzed the coverage and connectivity of a UV network combined with a designed node model and specific communication mode. The main contributions of this article are as follows:

1) A two-dimensional network coverage model was mathematically analyzed based on the coverage evaluation parameters. Furthermore, expressions for the network coverage and connectivity were derived separately.
2) The effects of the transceiver elevation combination, number of nodes, data rate, and transmission power on the network coverage were analyzed, and the communication parameters were optimized to match different network scenarios.
3) Based on a designed terminal, a coverage evaluation experiment was performed on a four-node UV network. The experimental results were compared with the simulation results, and the differences were analyzed.

The remainder of this article is organized as follows. Section II introduces the communication modes coverage evaluation parameters and the designed node model. Section III explains the derivation of the network coverage performance. Section IV discusses the simulation results to analyze the influence of different communication parameters on network coverage. Section V is discusses the four-node UV network coverage

Manuscript received 30 November 2023; revised 14 January 2024; accepted 25 January 2024. Date of publication 1 February 2024; date of current version 13 February 2024. This work was supported by the National Natural Science Foundation of China under Grants 62171463 and 62271502. *(Corresponding author: Jianhua Li.)*

The authors are with the College of Communication Engineering, Army Engineering University of PLA, Nanjing 210007, China (e-mail: ljhice@163.com).

Digital Object Identifier 10.1109/JPHOT.2024.3361215

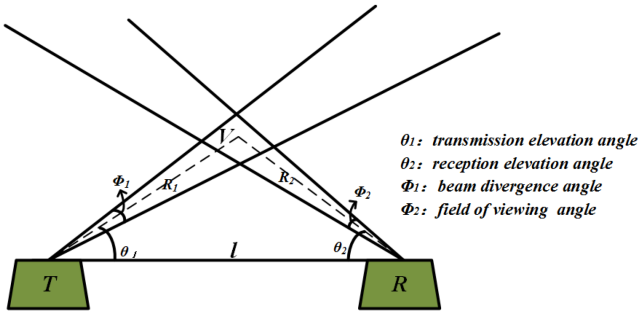

Fig. 1. UV NLOS scattering model.

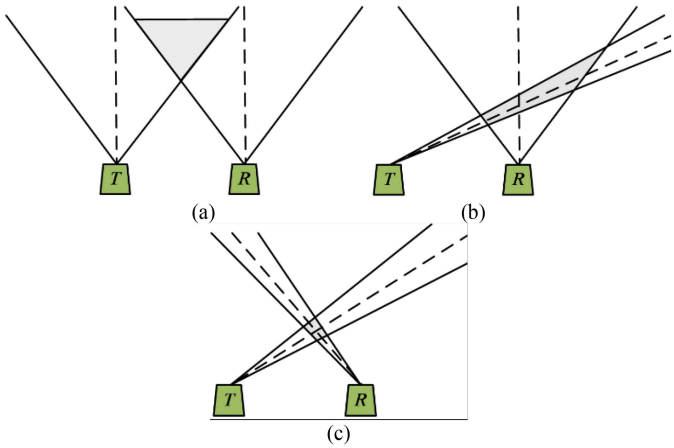

Fig. 2. UV NLOS communication modes: (a) NLOS-a, (b) NLOS-b, and (c) NLOS-c.

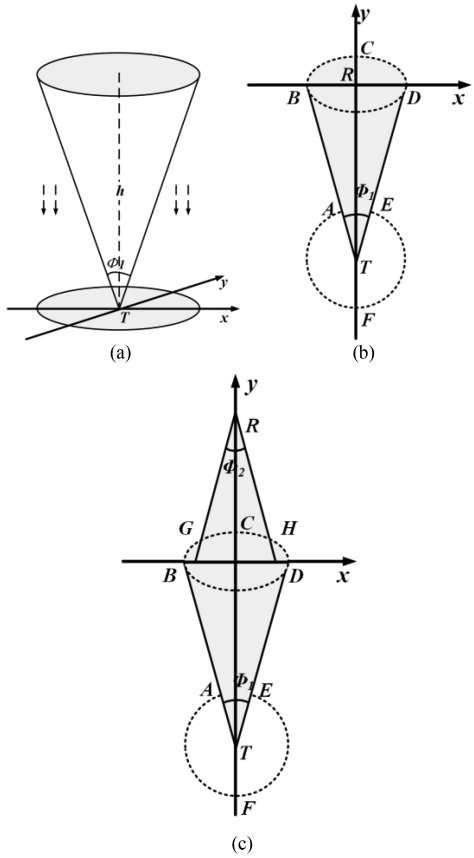

Fig. 3. UV NLOS coverage models: (a) NLOS-a, (b) NLOS-b, and (c) NLOS-c.

evaluation experiment. Finally, we summarize the conclusions of this study and discuss future prospects in Section VI.

II. Preliminaries

A. Communication Modes

The UV NLOS communication model is shown in Fig. 1 [11], where V is the effective scatterer, l is the communication distance, and r_1 and r_2 are the distance from the transmitter T to V and the distance from V to the receiver R, respectively. The light signal was transmitted into the atmosphere at T and received at R after being scattered by V.

As shown in Fig. 2, the communication can be divided into three modes, according to the combination of angles θ_1 and θ_2: NLOS-a for vertical transmission and vertical receiving, NLOS-b for nonvertical transmission and vertical receiving, and NLOS-c for nonvertical transmission and nonvertical receiving. These correspond to the three coverage models shown in Fig. 3, and a rectangular coordinate system was established [12].

In NLOS-a, the forward and backward scattering of the emitting beam are the same, and its coverage is a circular area. Compared with NLOS-a and NLOS-b, a communication system using the NLOS-c mode has a larger bandwidth, smaller delay, and longer communication distance, and its communication performance is evidently better [12]; however, it can only receive signals in a fixed direction. Because the performance of different UV communication modes varies greatly, the selection of modes and elevation combinations must be prioritized in a UV communication network.

B. Coverage Evaluation Parameters

The goal of coverage evaluation is to optimize and improve the network node resources for complete coverage over the regions of interest (ROIs), which is the premise and foundation for the establishment of a communication network [13]. The evaluation parameters of network coverage primarily include the coverage and connectivity [14]:

1) Effective Coverage Area: The effective coverage area refers to the unified coverage of all nodes, that is, the remaining area of the coverage of all nodes except the overlapping regions [15].

2) Connectivity: M-connectivity evaluates the degree of connectivity among network nodes. In an m-connectivity network, any node in the network has at least m adjacent nodes that can communicate directly [16]. The higher the connectivity, the more robust the network.

C. Node Model

To comprehensively utilize the advantages of the NLOS-c mode with a large bandwidth, small delay, and strong directivity and the reception omnidirectionality of the NLOS-b mode, a

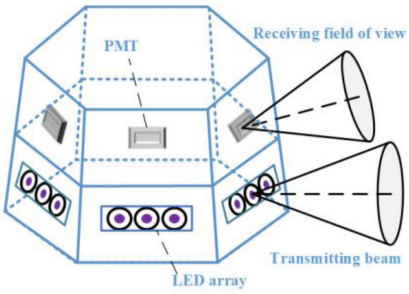

Fig. 4. Node model of the designed hexahedral UV terminal.

TABLE I
UV COMMUNICATION PARAMETERS

Parameter	Value
speed of light c	3.0×10^{8} m/s
wavelength λ	250 nm
quantum efficiency of filter and photodetector η	0.045
bit error rate P_e	10^{-6}
data rate R_d	50 kbps
Planck constant h	6.62×10^{-34} J·s
transmission power P_t	0.5 W
transmission elevation angle θ_1	10°–90°
reception elevation angle θ_2	10°–90°
beam divergence angle Φ_1	17°
field of view angle Φ_2	30°

hexahedral UV terminal model with directional transmission and omnidirectional reception was creatively designed, as shown in Fig. 4. Each side had separate transmission and reception devices. A UV light-emitting diode (LED) array was used to increase the transmission power and improve communication performance. Furthermore, each side of the terminal was equipped with a photomultiplier (PMT) to increase the efficiency of detection and achieve omnidirectional reception.

III. NETWORK COVERAGE ANALYSIS

A. Node Communication Distance

According to our previous study [17], the UV communication distance for on–off keying (OOK) is as follows:

$$l_{OOK} = \sqrt[\alpha]{-\frac{\eta\lambda P_t}{hc\xi R_d \ln(2P_e)}}. \quad (1)$$

The loss exponent α and loss factor ξ are related to transceiver elevation combinations. R_d, P_e, P_t, c, h, λ, and η are defined in Table I

We determined the relationship between transceiver elevation angle and node communication distance, as shown in Fig. 5, for the UV communication parameters listed in Table I.

Fig. 5 demonstrates that the communication distance decreases with increasing transceiver elevation angle. Notably, a slight increase in the communication distance occurs as the transmission elevation angle increases from 40° to 50°. The

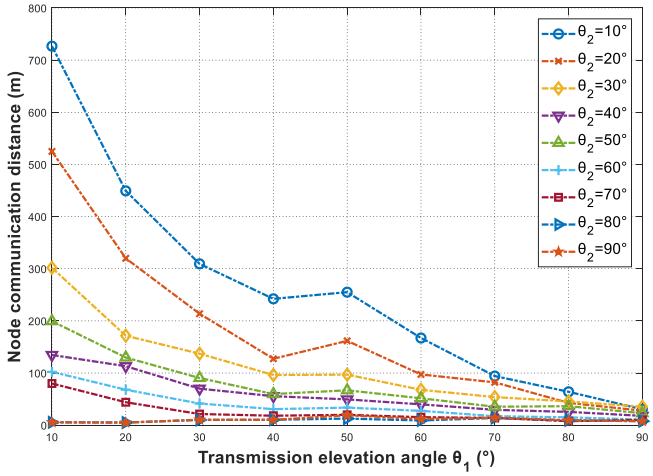

Fig. 5. Node communication distance versus transceiver elevation angle.

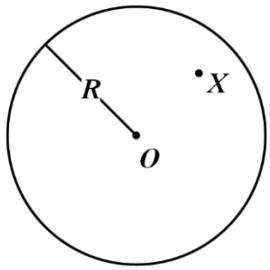

Fig. 6. Boolean coverage model: point X is considered covered when it lies within radius R and not covered when $d(O, X) \geq$ R.

distance gain caused by an increase in the effective scatterer with an increase in the angle is greater than the path loss in this case. As elevation angle continues to increase, the path loss increases constantly and the communication distance decreases accordingly.

B. Network Coverage Area

We used the Boolean model to study the coverage [18]. The Boolean coverage model is also known as the "0-1 model" because it has only two states: covered and not being covered, as shown in Fig. 6. Assuming that the coverage radius of node O is R, the coverage rate $p(X)$ of node O at a certain point X is given as

$$p(X) = \begin{cases} 1, & d(O,X) < R \\ 0, & d(O,X) \geq R \end{cases}, \quad (2)$$

where $d(O, X)$ represents the distance between nodes O and X.

1) UV Node: Without loss of generality, one side of the hexahedral node model described in Section II-C was randomly selected for the UV node coverage analysis. A single-side coverage model of the UV node was established, as shown in Fig. 7. Here, TO is the central axis; T and O are the vertex and center of the emitting light cone, respectively; Φ_1 is the beam divergence angle; θ_1 is the transmission elevation angle; and R_1 is the communication radius of the transmitter. The projection of

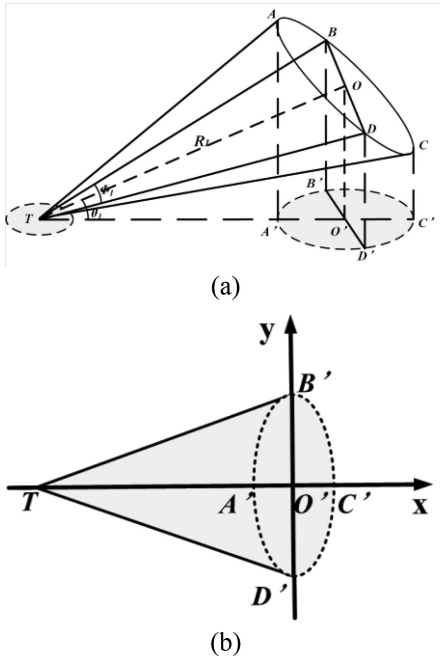

Fig. 7. Single-side coverage model of the UV node: (a) stereogram and (b) projection.

the emitting light cone is shown in Fig. 7(b), and a rectangular coordinate system was established with O' as the origin.

From the geometric relationship between $\triangle TAA'$, $\triangle TOD$ and $\triangle TOO'$, we obtain

$$\begin{cases} TO' = R_1 \cos\theta_1 \\ TA' = R_1 \cos\left(\theta_1 + \frac{\phi_1}{2}\right) \\ OD = O'D' = R_1 \tan\left(\frac{\phi_1}{2}\right) \\ O'A' = R_1\left(\cos\theta_1 - \cos\left(\theta_1 + \frac{\phi_1}{2}\right)\right) \\ B'D' = 2O'D' = 2R_1 \tan\left(\frac{\phi_1}{2}\right) \end{cases}, \tag{3}$$

where

$$R_1 = \frac{\sin\theta_2}{\sin\left(\theta_1 + \theta_2\right)} l. \tag{4}$$

The triangular area $S_{\triangle B'TD'}$ is given as

$$S_{\triangle B'TD'} = \frac{1}{2} B'D' \cdot TO' = R_1^2 \cos\theta_1 \tan\left(\frac{\phi_1}{2}\right). \tag{5}$$

The elliptical area $S_{\bigcirc B'C'D'A'}$ is given as

$$\begin{aligned} S_{\bigcirc B'C'D'A'} &= \pi O'D' \cdot O'A' \\ &= \pi R_1^2 \tan\left(\frac{\phi_1}{2}\right)\left(\cos\theta_1 - \cos\left(\theta_1 + \frac{\phi_1}{2}\right)\right), \end{aligned} \tag{6}$$

where $O'D'$ and $O'A'$ are the semi-major and semi-minor axes of the ellipse, respectively.

Forward scattering is evidently stronger than back scattering in the NLOS-c mode; therefore, the coverage of forward scattering is the primary factor to be considered. The coverage

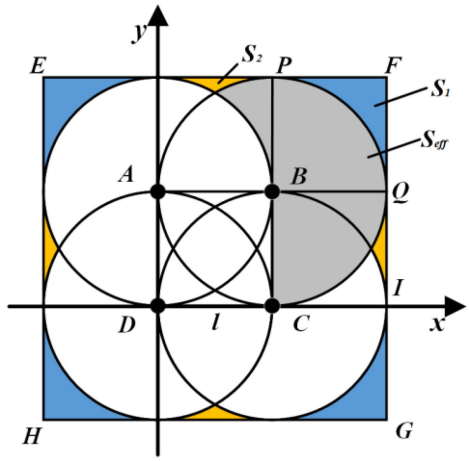

Fig. 8. Four-node square network deployment.

$S_{TB'C'D'}$ from the single-side coverage model of the UV node is given as

$$S_{TB'C'D'} = S_{\triangle B'TD'} + \frac{1}{2} S_{\bigcirc B'C'D'A'}. \tag{7}$$

2) UV Network: The square network deploys nodes efficiently and is convenient for networking, which is conducive to the rapid formation of network topology. Currently, square network deployment is widely used when the nodes are arranged to form communication networks [19], [20]. Therefore, the coverage and connectivity of the UV network were analyzed on the basis of square networks in this study. The following assumptions were made during the performance analysis:

a) All UV nodes have the same structure and communication parameter settings, including transmission power, data rate, and communication angles.
b) The analysis is based on a two-dimensional plane. The communication distance of the UV node is l, and the coverage of the directional transmission of the multi-sides is a circular region with radius l.
c) Each node can be considered as an integrated transceiver terminal with both transmission and reception devices.

The four-node square network deployment is shown in Fig. 8 with a network side length EF of $3l$. Further, a rectangular coordinate system was established, with point D as the origin.

The equation of circle A is given as

$$x^2 + (y - l)^2 = l^2. \tag{8}$$

The equation of line EF is given as

$$y = 2l. \tag{9}$$

The effective coverage of the four-node square network is the union of the coverage of all nodes, which is expressed as

$$S_{4-eff} = S_{\square EFGH} - 4S_1 - 4S_2, \tag{10}$$

where S_1 and S_2 are shown in Fig. 8(blue and yellow areas, respectively) and the square area $S_{\square EFGH}$ with side length $3l$ is given as

$$S_{\square EFGH} = 9l^2. \tag{11}$$

Based on (8) and (9), the following can be obtained:

$$S_2 = 2\int_0^{1/2} 2l - \left(l + \sqrt{l^2 - x^2}\right)$$
$$dx = \left(1 - \frac{1}{6}\pi - \frac{\sqrt{3}}{4}\right) l^2. \tag{12}$$

The sector area S_{PBQ} is given as

$$S_{PBQ} = \frac{1}{4} S_{\bigcirc B} = \frac{1}{4}\pi l^2, \tag{13}$$

thus,

$$S_1 = S_{\square PBQF} - S_{PBQ} = l^2 - \frac{1}{4}\pi l^2. \tag{14}$$

According to (10), (11), (12), and (14), we obtain

$$S_{4-eff} = \left(1 + \sqrt{3} + \frac{5}{3}\pi\right) l^2. \tag{15}$$

When any UV node is added to a square network, the increased effective coverage area is S_{eff} (gray area in Fig. 8), which is also the maximum effective coverage area achieved by a single communication node in the network (except the boundary node).

The sector area S_{PQCB} is given as

$$S_{PQCB} = \frac{1}{2} S_{\bigcirc B} = \frac{1}{2}\pi l^2. \tag{16}$$

By symmetry,

$$S_{eff} = S_{PQCB} + (S_1 - S_2) = \frac{5}{12}\pi l^2 + \frac{\sqrt{3}}{4} l^2. \tag{17}$$

C. Network Connectivity

The connectivity analysis was based on a two-dimensional area C, with area S_{ROI}. In a square network, n nodes are evenly deployed. The probability density function of the square network is given as

$$U(t_x, \varphi_x) = \begin{cases} \frac{n}{S_{ROI}} & (t_x, \varphi_x) \in C \\ 0 & \text{else} \end{cases}. \tag{18}$$

As shown in Fig. 9, the coverage $S_{node}(t_x, \varphi_x)$ of any node $x(t_x, \varphi_x)$ is a circular area, with (t_x, φ_x) as the center and l as the radius:

$$(t\cos\varphi - t_x\cos\varphi_x)^2 + (t\sin\varphi - t_x\sin\varphi_x)^2 = l^2. \tag{19}$$

When the distance d between $x(t_x, \varphi_x)$ and origin O is greater than or equal to l, as in Fig. 9(a), from (19) we obtain

$$\begin{cases} \varphi_1 = \arcsin\left(\frac{t_x \sin\varphi_x}{t_x}\right) - \arcsin\left(\frac{l}{t_x}\right) \\ \varphi_2 = \arcsin\left(\frac{t_x \sin\varphi_x}{t_x}\right) + \arcsin\left(\frac{l}{t_x}\right) \\ t_1 = t_x\cos\varphi_x\cos\varphi + t_x\sin\varphi_x\sin\varphi - \\ \sqrt{(t_x\cos\varphi_x\cos\varphi + t_x\sin\varphi_x\sin\varphi)^2 - (t_x^2 - l^2)} \\ t_2 = t_x\cos\varphi_x\cos\varphi + t_x\sin\varphi_x\sin\varphi + \\ \sqrt{(t_x\cos\varphi_x\cos\varphi + t_x\sin\varphi_x\sin\varphi)^2 - (t_x^2 - l^2)} \end{cases}. \tag{20}$$

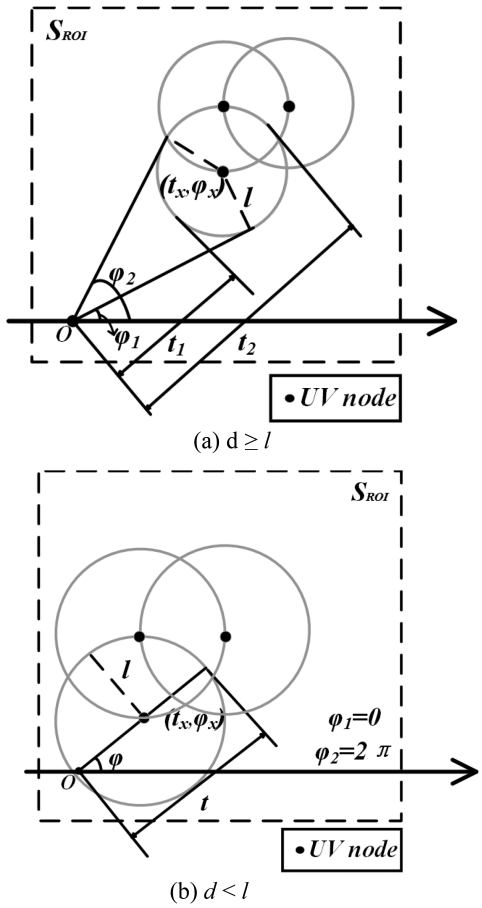

Fig. 9. Connectivity analysis diagram for distances d between point x and the origin O (a) $d > l$ and (b) $d < l$.

Here, φ_1 and φ_2 and t_1 and t_2 represent the upper and lower bounds of the integral area, respectively. When $d < l$, as in Fig. 9(b),

$$\begin{cases} \varphi_1 = 0 \\ \varphi_2 = 2\pi \\ t_1 = 0 \\ t_2 = t_x\cos\varphi_x\cos\varphi + t_x\sin\varphi_x\sin\varphi + \\ \sqrt{(t_x\cos\varphi_x\cos\varphi + t_x\sin\varphi_x\sin\varphi)^2 - (t_x^2 - l^2)} \end{cases}. \tag{21}$$

The probability $P(t_x, \varphi_x, l)$ that node $x(t_x, \varphi_x)$ has adjacent nodes is given as

$$P(t_x, \varphi_x, l) = \begin{cases} \int_{t_1}^{t_2} dt \int_{\varphi_1}^{\varphi_2} U(t\cos\varphi, t\sin\varphi) t d\varphi, & t_x \geq l \\ \int_{t_1}^{t_2} dt \int_{\varphi_1}^{\varphi_2} U(t\cos\varphi, t\sin\varphi) t d\varphi, & t_x < l \end{cases}. \tag{22}$$

The remaining nodes within the coverage of node $x(t_x, \varphi_x)$ obey the binomial distribution $Bin(n-1, P(t_x, \varphi_x, l))$; therefore, the probability that $x(t_x, \varphi_x)$ has m adjacent nodes is expressed as

$$P_m(t_x, \varphi_x, l) = \binom{n-1}{m} \cdot P(t_x, \varphi_x, l)^m \cdot$$
$$(1 - P(t_x, \varphi_x, l))^{n-1-m}. \tag{23}$$

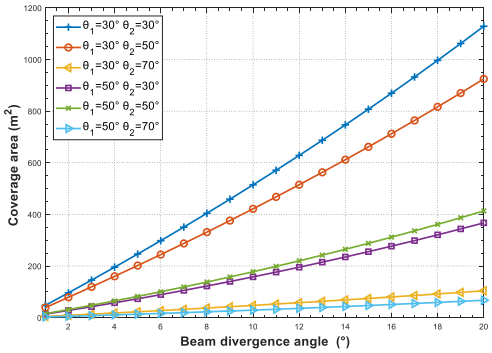

Fig. 10. Covered area versus divergence angle for different transceiver elevation combinations.

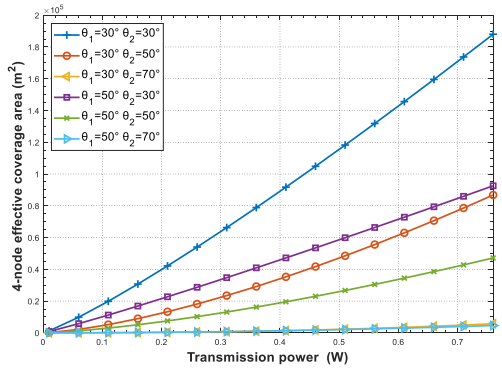

Fig. 11. Four-node effective coverage area versus transmission power for different transceiver elevation combinations.

Then, the probability that $x(t_x, \varphi_x)$ has more than m adjacent nodes is given as

$$P_{\geq m}(t_x, \varphi_x, l) = 1 - \sum_{s=0}^{m-1} \binom{n-1}{s} P(t_x, \varphi_x, l)^s \cdot (1 - P(t_x, \varphi_x, l))^{n-1-s}. \quad (24)$$

The probability that an arbitrary node has more than m adjacent nodes is given by

$$Q_{n,\geq m}(l) = \iint_{S_{ROI}} U(t\cos\varphi, t\sin\varphi) P_{\geq m}(t_x, \varphi_x, l) t d\varphi dt. \quad (25)$$

The probability that each node has more than m adjacent nodes is approximated as the probability of an m-connected network it and can be obtained as follows [21]:

$$P(C \text{ is } m-\text{connected}) \approx P(d_{\min} \geq m). \quad (26)$$

Hence, the probability of an m-connected network is expressed as

$$P(C \text{ is } m-\text{connected}) \approx (Q_{n,\geq m}(l))^n = \left(\iint_{S_{ROI}} U(t\cos\varphi, t\sin\varphi) P_{\geq m}(t_x, \varphi_x, l) t d\varphi dt \right)^n. \quad (27)$$

IV. Simulation and Analysis

A. Coverage Area

1) UV Node: According to the analysis in Fig. 5, large elevation angles shorten the communication distance and cannot be used in actual networking. Similarly, excessively small elevation angles cannot be used to achieve NLOS communication. Transmission elevation angles of 30° and 50° were selected for the simulation in this study. Generally, the beam divergence angle should not exceed 20° to avoid power diffusion of the UV emission beam.

Fig. 10 shows that the trends of the covered area of a single side of UV nodes with respect to the beam divergence angle Φ_1 are approximately identical for different transceiver elevation combinations. Therefore, with an increase in Φ_1, the coverage of the single side increases.

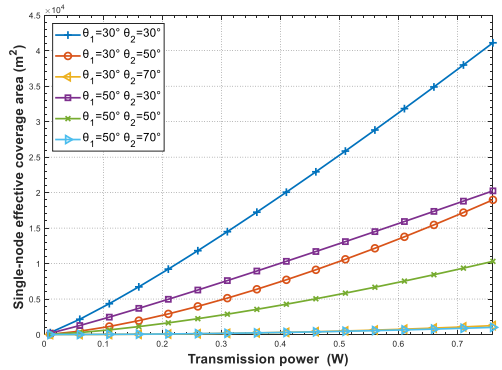

Fig. 12. Single-node effective coverage area versus transmission power for different transceiver elevation combinations.

Comparing the coverage horizontally reveals that, when Φ_1 remains the same, the smaller the transceiver elevation combination, the larger the coverage. When the transceiver elevation combination is 30°–30°, the coverage of a single side is 8.07 $\times$ 10^2 m^2, with a divergence angle of 15°, which is approximately 122.15% and 297.51% of those of the 30°–50° (6.61 $\times$ 10^2 m^2) and 50°–50° (2.71 $\times$ 10^2 m^2) transceiver elevation combinations, respectively.

2) UV Network: Figs. 11 and 12 show the four-node effective coverage area and single-node effective coverage area versus the transmission power P_t for varying transceiver elevation combinations, respectively. Similar trends are observed for both coverages: an increase in the communication distance leads to an increase in coverage as P_t increases.

Figs. 11 and 12 illustrate that the smaller the transceiver elevation angles, the faster the coverage increases with an increase in P_t. When the transceiver elevation combination is 30°–30°, the four-node effective coverage area is 1.15 $\times$ 10^5 m^2, with a transmission power of 0.5 W, which is approximately 257.84% and 197.25% of those of the 30°–50° (4.46 $\times$ 10^4 m^2) and 50°–30° (5.83 $\times$ 10^4 m^2) transceiver elevation combinations, respectively.

Figs. 13 and 14 show the four-node effective coverage area and single-node effective coverage area versus the data rate R_d for varying transceiver elevation combinations, respectively. As

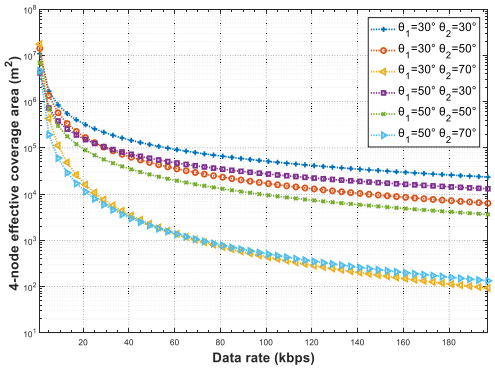

Fig. 13. Four-node effective coverage area versus data rate for different transceiver elevation combinations.

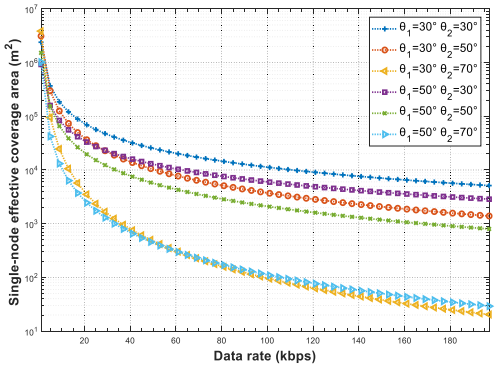

Fig. 14. Single-node effective coverage area versus data rate for different transceiver elevation combinations.

R_d increases, a decrease in the communication distance leads to a decrease in the coverage area.

By horizontally comparing the results in Figs. 13 and 14, we deduced that the choice of transceiver elevation angles has a great impact on the effective coverage area with the same R_d. Fig. 14 shows that the single-node effective coverage area increases by approximately 81.86% from 50°–50° (5.83×10^3 m^2) to 30°–50° (1.06×10^4 m^2), and by 343.26% from 50°–50° to 30°–30° (2.58×10^4 m^2) when R_d is 50 kbps.

The maximum effective coverage ratio of UV node η_{eff} was defined as the ratio of the maximum effective coverage area to the coverage area of a single node [19], which is given as

$$\eta_{eff} = \frac{S_{eff}}{S_{node}} = 55.45\%. \tag{28}$$

In the area S_{ROI} shown in Fig. 15, the minimum number of nodes n_{min} required to achieve completely seamless coverage when deploying a square UV network is

$$n_{min} = \frac{S_{ROI}}{S_{eff}} = \frac{S_{ROI}}{\eta_{eff} \cdot S_{node}}. \tag{29}$$

Equation (29) provides a theoretical reference for the number of nodes required for the deployment of UV networks. Assuming that S_{ROI} is a square area with a side length of 1.0×10^3 m, to achieve full coverage of the target area, the number of UV nodes

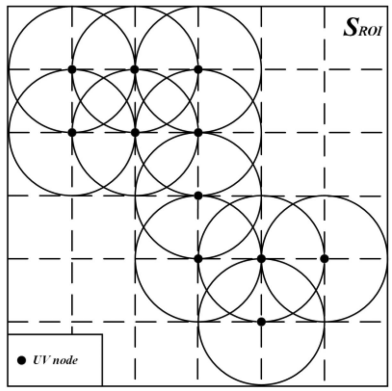

Fig. 15. Square network deployment of UV nodes.

n_{min} is theoretically required to be 96 with a transceiver elevation combination of 30°–50°. However, owing to the boundary effect, the UV node required in actual deployment is generally greater than the theoretical value.

B. Connectivity

According to the analysis in Section IV-A, the effective coverage area of UV nodes for actual communication networks are far less than those in cases where the transceiver elevation angles are large. To obtain better communication coverage and achieve NLOS communication, four transceiver elevation combinations were selected: 30°–30°, 30°–50°, 50°–30°, and 50°–50°. The network connectivity simulations were performed in a square area with a side length of 1.0×10^3 m.

1) Number of Nodes: Fig. 16 shows that the UV network connectivity has similar growth trends with the number of nodes n under different transceiver elevation combinations (R_d = 50 kbps; $P_t = 0.5$ W). Initially, a near-linear trend is observed in the connectivity growth with n as more nodes are deployed. With a continuous increase in the number of nodes, the connectivity growth decreases and the connectivity gradually approaches 100%. Owing to the fact that a large number of node resources are needed to increase the connectivity to 100%, 90% connectivity is considered as the evaluation standard of connectivity in actual UV networking.

Fig. 16 illustrates the more stringent conditions for achieving a multi-connected network under the same communication parameters for larger multi-connectivities. In the 30°–30° transceiver elevation combination, the number of nodes required to reach 90% connectivity increases by 51.02% for a two-connected network (73 nodes) compared to a one-connected network (48), and the number of nodes increases by 106.12% for three-connectivity (101).

The two-connected network is robust, and the channel parameter requirements are less stringent than multi-connectivities. Horizontal comparison reveals that the smaller the transceiver elevation combination, the smaller the number of nodes required to form a two-connected network. A total of 73 nodes must be deployed to the network to achieve two-connectivity with the 30°–30° transceiver elevation combination. The number of nodes required with 50°–30° and 50°–50° transceiver elevation

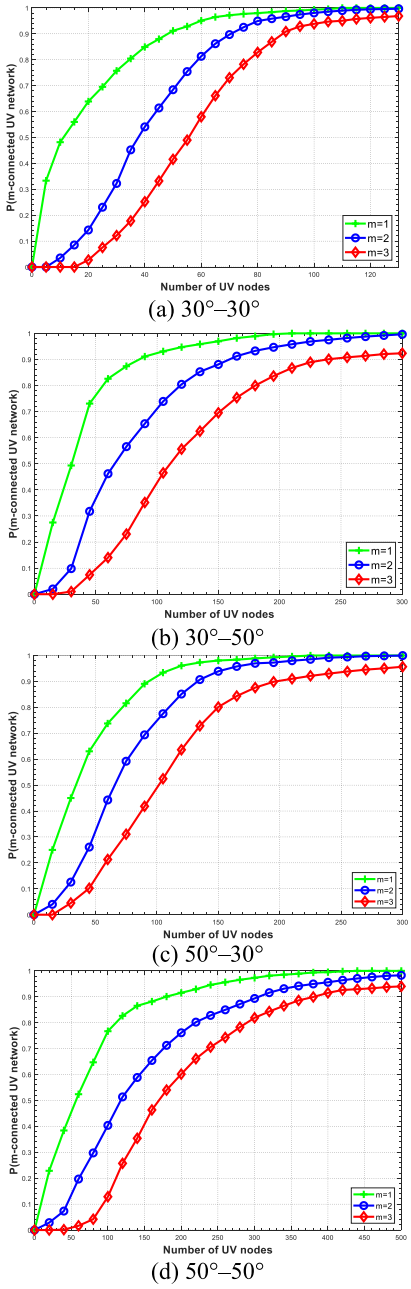

Fig. 16. Network connectivity versus number of nodes for various multi-connectivities, with transceiver elevation angle combinations (a) 30°–30°, (b) 30°–50°, (c) 50°–30°, and (d) 50°–50°.

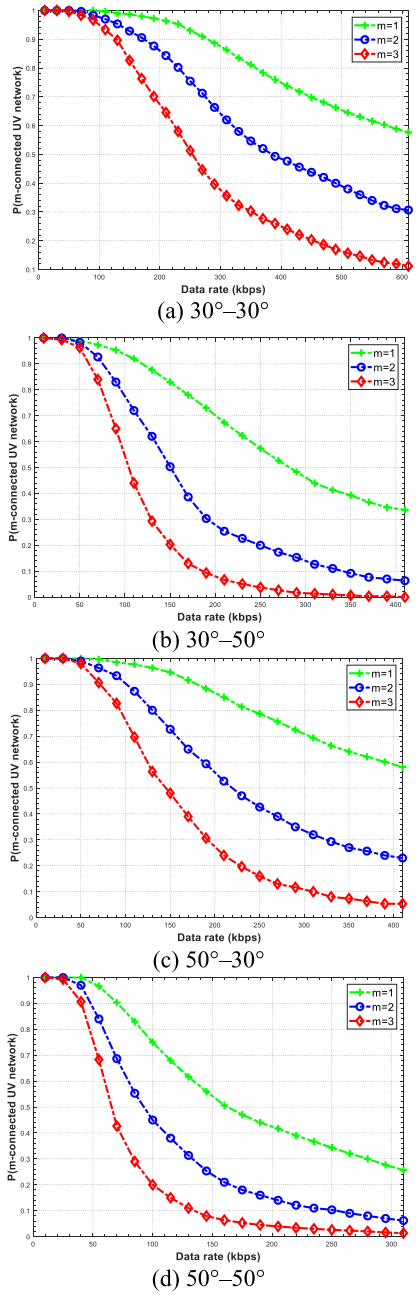

Fig. 17. Network connectivity versus data rate for various multi-connectivities, with transceiver elevation combinations (a) 30°–30°, (b) 30°–50°, (c) 50°–30°, and (d) 50°–50°.

combinations are 135 and 301, respectively, which are approximately 183.78% and 408.10% of that of the 30°–30° elevation combination.

2) Data Rate: Fig. 17 shows the connectivity versus data rate R_d for different transceiver elevation combinations ($n = 300$, $P_t = 0.5$ W). The results indicate that the network connectivity decreases with an increase in R_d. The higher the value of m in the connected network, the lower the supported R_d. The data rate supported by the one-connected network is 117 kbps with the 30°–50° transceiver elevation combination, and the rates supported by the two- and three-connected networks are 73 kbps and 58 kbps, respectively, which are reduced by 37.61% and 50.43% compared to that of the one-connected state.

3) Transmission Power: Fig. 18 shows the connectivity versus transmission power P_t for different transceiver elevation combinations ($n = 300$, $R_d = 50$ kbps). The network connectivity increases with increasing P_t and gradually approaches 100%. For the same transceiver elevation combinations, multi-connected states require a higher transmission power. Compared to the one-connected state (0.24 W), the transmission power P_t of the network increases by 41.66% for the two-connected state (0.34 W) and by 75.00% for a three-connected state (0.42 W),

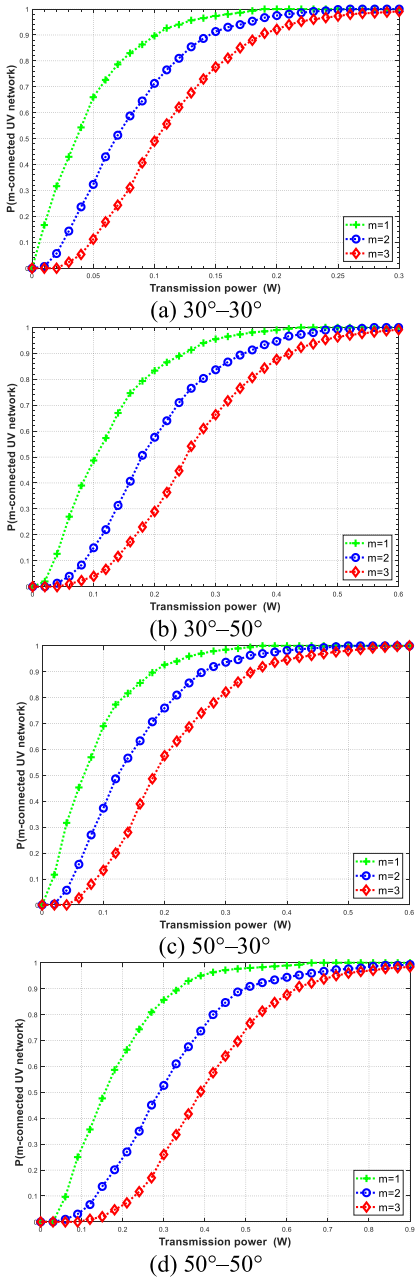

Fig. 18. Network connectivity versus transmission power for various multi-connectivities, with transceiver elevation combinations (a) 30°–30°, (b) 30°–50°, (c) 50°–30°, and (d) 50°–50°.

with the 30°–50° transceiver elevation combination, as shown in Fig. 18(b).

Comparing Figs. 16–18 reveals that the bigger the transceiver elevation combination, the more stringent the communication parameters (number of nodes, data rate, and transmission power) required by the connected UV network. Therefore, the selected elevation combination should be as small as possible for NLOS communication in actual UV networking.

Overall, compared to the blind coverage area, the isolation of communication terminals causes more serious damage to the network performance. Therefore, it is appropriate to construct

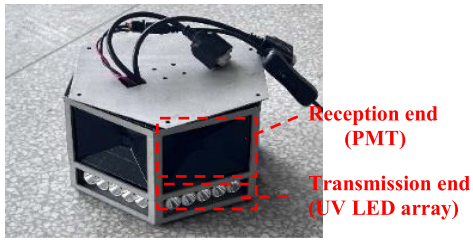

Fig. 19. UV communication terminal for experiments.

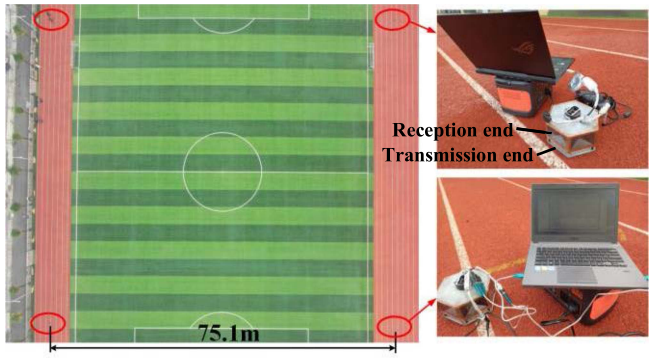

Fig. 20. Scene of the four-node UV network experiment.

a UV network with two-connectivity and one coverage area for practical applications.

V. Experiment and Analysis

We conducted a coverage evaluation experiment with a four-node UV network based on the designed terminals. The experimental results were compared with the simulation results, and the differences were analyzed.

A. Experimental Conditions

According to the node model described in Section II-C, a hexagonal terminal model was designed as shown in Fig. 19; each side had separate transmission and reception devices. A 1 × 5 UV LED array was used at the transmission end to improve communication distance and the total power of a single side was 0.5 W. The PMT was used at the reception end, with a response time at the nanometer level. The communication mode of NLOS-c with OOK modulation was used for each side with an elevation angle combination of 30°–50°.

Each node can be considered an integrated transceiver terminal with both transmission and reception devices. In the communication network, a UV networking protocol previously proposed by our team was used [22], and each node could transmit and receive data. The four terminals were deployed according to a square network. The experiment scene is shown in Fig. 20.

B. Experimental Results

The measured communication distance between terminals was 75.1 m, and the effective coverage area of the four-node network was 4.48×10^4 m^2. Compared to the simulation results,

where the coverage area of the four-node network was 4.62×10^4 m^2 under the same parameter conditions (Fig. 11), the area in the experiments was slightly smaller.

Although the "solar blind" UV band was selected, a small amount of background interference was still present in the experiments. This background noise was ignored in the simulations, thus the effective coverage area in the simulations was higher.

VI. Conclusion

UV network has great potential in covert communication and has high prospects for application in the complex electromagnetic environment. In this study, we systematically evaluated UV network coverage based on an NLOS channel. A two-dimensional network coverage model was established, which was combined with a designed node model and a specific communication mode. Furthermore, the expressions of the effective coverage area and connectivity were derived mathematically. Subsequently, the effects of communication parameters on the network coverage performance were analyzed. We observed that the bigger the transceiver elevation combination, the more stringent the communication parameters (number of nodes, data rate, and transmission power) required by the UV network coverage. Finally, a coverage evaluation experiment with a four-node network was conducted. The experimental results were consistent with the simulation results. Thus, comprehensive consideration of the network coverage and connectivity can guide node deployment in practical UV networking.

Network life is another factor affecting coverage performance. Owing to the limitation of the energy of the node, stable and efficient strategies are urgently needed to improve the energy utilization efficiency of the nodes and extend the working lives of UV networks as much as possible. Therefore, in subsequent research, we aim to examine the rational utilization of energy in the construction of UV networks.

Disclosures

The authors declare no conflicts of interest.

Data Availability

The data underlying the results presented in this article are not publicly available at this time but may be obtained from the authors upon reasonable request.

References

[1] A. Vavoulas, H. G. Sandalidis, N. D. Chatzidiamantis, Z. Xu, and G. K. Karagiannidis, "A survey on ultraviolet c-band (UV-C) communications," *IEEE Commun. Surveys Tut.*, vol. 21, no. 3, pp. 2111–2133, thirdquarter 2019, doi: 10.1109/COMST.2019.2898946.

[2] L. Wang et al., "Full-duplex wireless deep ultraviolet light communication," *Opt. Lett.*, vol. 47, no. 19, pp. 5064–5067, 2022.

[3] A. Refaai, M. Abaza, M. S. El-Mahallawy, and M. H. Aly, "Performance analysis of multiple NLOS UV communication cooperative relays over turbulent channels," *Opt. Exp.*, vol. 26, no. 16, pp. 19972–19985, 2018, doi: 10.1364/OE.26.019972.

[4] G. Chen, Z. Xu, H. Ding, and B. M. Sadler, "Path loss modeling and performance trade-off study for short-range non-line-of-sight ultraviolet communications," *Opt. Exp.*, vol. 17, no. 5, pp. 3929–3940, 2009.

[5] R. J. Drost and B. M. Sadler, "Survey of ultraviolet non-line-of-sight communications," *Semicond. Sci. Technol.*, vol. 29, no. 8, 2014, Art. no. 084006, doi: 10.1088/0268-1242/29/8/084006.

[6] J. Roselin et al., "Maximizing the wireless sensor networks lifetime through energy efficient connected coverage," *Ad Hoc Netw.*, vol. 62, no. 62, pp. 1–10, 2017, doi: 10.1016/j.adhoc.2017.04.001.

[7] T. Zhao, Y. Gao, and Y. Zhang, "An area coverage algorithm for non-line-of-sight ultraviolet communication network," *Photon. Netw. Commun.*, vol. 32, no. 2, pp. 269–280, 2016.

[8] X. Ke and Y. Wu, "Diamond communication network design for the non-line-of-sight ultraviolet channel model," *Opt. Eng.*, vol. 60, no. 3, 2021, Art. no. 036104, doi: 10.1117/1.OE.60.3.036104.

[9] A. Vavoulas, H. G. Sandalidis, and D. Varoutas, "Connectivity issues for ultraviolet UV-C networks," *J. Opt. Commun. Netw.*, vol. 3, no. 3, pp. 199–205, 2011.

[10] T. Zhao, Y. Xie, and Y. Zhang, "Connectivity properties for UAVs networks in wireless ultraviolet communication," *Photon. Netw. Commun.*, vol. 35, pp. 316–324, 2018.

[11] H. Tadayyoni, M. H. Ardakani, A. R. Heidarpour, and M. Uysal, "Ultraviolet communications for unmanned aerial vehicle networks," *IEEE Wireless Commun. Lett.*, vol. 11, no. 1, pp. 178–182, Jan. 2022.

[12] A. Refaai, M. Abaza, M. S. El-Mahallawy, and M. H. Aly, "Performance analysis of multiple NLOS UV communication cooperative relays over turbulent channels," *Opt. Exp.*, vol. 26, no. 16, pp. 19972–19985, 2018.

[13] H. H. Yang and T. Q. S. Quek, "SIR coverage analysis in cellular networks with temporal traffic: A stochastic geometry approach," *IEEE Trans. Wireless Commun.*, 2018, early access, doi: 10.48550/arXiv.1801.09888.

[14] S. Debnath, "Network coverage using MI waves for underwater wireless sensor network in shadowing environment," *IET Microw. Antennas Propag.*, vol. 15, no. 9, pp. 1035–1041, 2021, doi: 10.1049/mia2.12113.

[15] Y. Stergiopoulos, M. Thanou, and A. Tzes, "Distributed collaborative coverage-control schemes for non-convex domains," *IEEE Trans. Autom. Control*, vol. 60, no. 9, pp. 2422–2427, Sep. 2015, doi: 10.1109/TAC.2015.2409903.

[16] A. Al-Dulaimi, S. Mumtaz, S. Al-Rubaye, S. Zhang, and C.-L. I, "A framework of network connectivity management in multi-clouds infrastructure," *IEEE Wireless Commun.*, vol. 26, no. 3, pp. 104–110, Jun. 2019.

[17] C. Li, J. Li, Z. Xu, and J. Wang, "Study on the k-connectivity of UV communication network under the node distribution of RWP mobility model in the arbitrary polygon area," *IEEE Photon. J.*, vol. 12, no. 4, Aug. 2020, Art. no. 7903912, doi: 10.1109/JPHOT.2020.3003896.

[18] K. Chakrabarty, S. S. Iyengar, H. Qi, and E. Cho, "Grid coverage for surveillance and target location in distributed sensor networks," *IEEE Trans. Comput.*, vol. 51, no. 12, pp. 1448–1453, Dec. 2002.

[19] L. Wang, Y. Li, and Z. Xu, "On connectivity of wireless ultraviolet networks," *J. Opt. Soc. Am. A Opt. Image Sci. Vis.*, vol. 28, no. 10, pp. 1970–1978, 2011, doi: 10.1364/JOSAA.28.001970.

[20] H. Qin, Y. Zuo, F. Li, R. Cong, L. Meng, and J. Wu, "Noncoplanar geometry for mobile NLOS MIMO ultraviolet communication with linear complexity signal detection," *IEEE Photon. J.*, vol. 9, no. 5, Oct. 2017, Art. no. 7906012, doi: 10.1109/JPHOT.2017.2742544.

[21] A. Vavoulas, H. G. Sandalidis, and D. Varoutas, "Node isolation probability for serial ultraviolet UV-C multi-hop networks," *J. Opt. Commun. Netw.*, vol. 3, no. 9, pp. 750–755, 2011, doi: 10.1364/JOCN.3.000750.

[22] C. Li, Z. Xu, and J. Wang, "Ultraviolet random access collaborative networking protocol based on time division multiple access," *J. Opt. Comm. Netw.*, vol. 15, no. 6, pp. 393–403, 2023, doi: 10.1364/JOCN.479471.